第37卷第8期 无 机 化 学 学 报 Vol.37 No.8
2021年8月 CHINESE JOURNAL OF INORGANIC CHEMISTRY 1475-1481

一锅法可控合成金属有机框架材料Mn-荧光素用于核磁共振/荧光成像

高雪川*,[1] 张 曼[1] 孙旭建[1] 王跃武[2]
([1]内蒙古工业大学化工学院,呼和浩特 010051)
([2]内蒙古医科大学新药安全评价研究中心,呼和浩特 010010)

摘要: 通过一锅法,首次将核磁共振成像试剂Mn^{2+}和荧光成像试剂荧光素(FSD)自组装于一个简单的金属有机框架材料(Mn-FSD)上。实验结果表明,Mn-FSD的粒径可被控制在微纳米水平内并进行生物成像。体外和体内实验结果证实,Mn-FSD可在细胞和裸鼠中显示强绿色荧光。同时,Mn-FSD表现出较高的弛豫值(r_1=4.95 L·mmol^{-1}·s^{-1})。

关键词: 金属有机框架材料; 可控合成; 荧光成像; 核磁共振成像; 一锅法
中图分类号: O614.71+1 **文献标识码:** A **文章编号:** 1001-4861(2021)08-1475-07
DOI: 10.11862/CJIC.2021.156

Controllable Synthesis of Metal-Organic Frameworks Mn-Fluorescein in One Pot for Magnetic Resonance/Optical Imaging

GAO Xue-Chuan*,[1] ZHANG Man[1] SUN Xu-Jian[1] WANG Yue-Wu[2]
([1]*College of Chemical Engineering, Inner Mongolia University of Technology, Hohhot* 010051, *China*)
([2]*The Center for New Drug Safety Evaluation and Research of Inner Mongolia Medical University, Hohhot* 010110, *China*)

Abstract: Through the one-pot method, for the first time, the NMR imaging reagent Mn^{2+} and the fluorescence imaging reagent fluorescein (FSD) were self-assembled on a simple metal organic framework (Mn-FSD). Fortunately, the particle size of as-obtained Mn-FSD can be controlled to the micro-nano level for bioimaging. The *in vitro* and *in vivo* outcomes confirm that Mn-FSD can show strong green fluorescence in cells and in nude mice. Simultaneously, Mn-FSD exhibited high relaxivity values (r_1=4.95 L·mmol^{-1}·s^{-1}).

Keywords: metal-organic framework; controllable synthesis; fluorescence imaging; magnetic resonance imaging; one-pot method

0 Introduction

Metal-organic frameworks (MOFs) are fascinating porous materials self-assembled from inorganic nodes and organic ligands, which attracted extensive attentions owing to their tunable porous structures, designable structure, large surface area, customizable chemistry, biodegradable and biocompatibility[1-5]. Benefiting from these intriguing properties, metal-organic frameworks (MOFs) have been widely used in various fields, such as luminescence, sensing, batteries, supercapacitors, gas storage, gas separation, catalysis, drug delivery and bioimaging[6-10]. For bioimaging, several MOFs have been constructed and explored for optical imaging (OI) and magnetic resonance imaging (MRI). For example, Chen group fabricated a novel core-shell PB@MIL-

收稿日期:2021-01-26。收修改稿日期:2021-05-11。
内蒙古自治区自然科学基金(No.2019BS02010)、内蒙古自治区高等学校科学技术研究项目(No.NJZY19073)和内蒙古工业大学博士启动基金(No.BS201909)资助。
*通信联系人。E-mail:cexcgao@imut.edu.cn

100 (Fe) with magnetic resonance and optical dual-model imaging capabilities[11]. Tang group designed and introduced an UCNP@Fe-MIL-101-NH_2@PEG@FA core-shell structure that are certainly capable of fluorescent/magnetic dual-modal imaging[12]. Our group also fabricated a smart MOF platform (Fe-MIL-53-NH_2-FA-5-FAM/5-FU) for magnetic resonance/optical imaging and targeted drug delivery[13]. However, such materials usually have complicated structure and require multi-step synthesis. Combining MRI and OI into one MOFs via one-pot method remains challenging and relatively unexplored.

In this study, micro-nano Mn-FSD was achieved successfully by one-pot method using glucose and polyvinyl pyrrolidone (PVP) as modulators. It is important to note that MRI and OI capacities are integrated into a simple MOFs firstly in this work, which is self-assembled from Mn^{2+} and fluorescein (FSD). As we know, Mn^{2+} based contrast agents are commonly used T_1 contrast agents, which are able to increase the longitudinal water proton relaxation rates, producing brighter image signals[14-16]. FSD can emit strong green fluorescence with high fluorescence quantum yield in aqueous media and has been widely used as a fluorescent probe[17-19]. Based on this, the Mn-FSD has the potential for MRI and OI. In the presence of PVP and glucose, the size of Mn-FSD can be adjusted into micro-nano range for biological application. As expected, Mn-FSD exhibited excellent fluorescence imaging capabilities in the cell and *in vivo*. Besides, Mn-FSD also displayed ideal magnetic resonance imaging abilities with high relaxivity values. All in all, this work integrated MRI and OL in one MOFs for the first time.

1 Experimental

1.1 Material and methods

All the starting reagents and solvents were acquired from commercial sources and used directly without further purification. Powder X-ray diffraction (XRD) patterns over the 2θ range from 5° to 80° were performed on an EMPYREAN PANALYTICAL apparatus using the Cu $K\alpha$ radiation (λ=0.154 059 8 nm) at a scanning rate of 2 (°)·min^{-1}. The voltage was 60 kV and the current was 55 mA. The morphology of the products was obtained using HITACHI-SU8220 scanning electron microscope (SEM) and FEI Tecnai G^2 F20 high-resolution transmission electron microscope (HRTEM). The accelerating voltage during testing is 20 and 200 kV, respectively. Energy-dispersive X-ray (EDX) mapping analysis was carried out on TEM. Photoluminescence (PL) spectra were collected on a Hitachi F-7000 fluorescence spectrophotometer. NEXUS-670 Fourier transform infrared spectrophotometer was used to record fourier transform infrared spectroscopy (FTIR) spectra. Thermogravimetric analysis (TGA) was performed from 0 to 800 ℃ using STA 449F^3-QMS 402D-IS50 thermal analyser under N_2 atmosphere. A laser scanning confocal microscope (Zeiss LSM 710) was used to bioimaging. UV-Vis spectra were recorded on a UV-3150 UV-visible spectrophotometer.

1.2 Construction of Mn-FSD with different sizes and morphologies

The Mn-FSD were prepared according to the previous work with some modifications[20]. In a normal procedure, 0.122 5 g $Mn(OAc)_2·4H_2O$, 0.8 g PVP and 0.8 g glucose were dissolved in 5 mL H_2O to obtain solution A, and 0.188 g fluorescein sodium salt (Na_2FSD) was dissolved in 4 mL methanol to obtain solution B. Subsequently, solution B was added to solution A and the mixture was heated at 90 ℃ for 24 h under hydrothermal condition. After that the mixture was cooled to room temperature and the product was collected and washed by centrifugation for several times as well as dried at 60 ℃. The obtained product was marked as Mn-FSD-1. 0.122 5 g $Mn(OAc)_2·4H_2O$ and 0.15 g PVP were dissolved in 5 mL H_2O to obtain solution A, and 0.188 g Na_2FSD and 0.15 g glucose were dissolved in 4 mL methanol to obtain solution B. Subsequently, solution B was added to solution A and the mixture was heated at 90 ℃ for 24 h under oil bath condition. The obtained product was marked as Mn-FSD-2. 0.122 5 g $Mn(OAc)_2·4H_2O$, 0.2 g PVP and 0.2 g glucose were dissolved in 5 mL H_2O to obtain solution A, and 0.188 g Na_2FSD was dissolved in 4 mL methanol to obtain solution B. Subsequently, solution B was added to solution

A and 4 mL DMF was added to the mixture. The mixture was heated at 90 ℃ for 24 h under hydrothermal condition. The obtained product was marked as Mn-FSD-3. 0.122 5 g $Mn(OAc)_2 \cdot 4H_2O$ and 0.15 g PVP were dissolved in 5 mL H_2O to obtain solution A, and 0.188 g Na_2FSD and 0.15 g glucose were dissolved in 4 mL methanol to obtain solution B. Subsequently, solution B was added to solution A and the mixture was heated at 90 ℃ for 24 h under hydrothermal condition. The obtained product was marked as Mn-FSD-4.

1.3 Cytotoxicity study

MTT method was used to evaluate the cell cytotoxicities of Mn-FSD-4. Briefly, HL-7702 cells and A549 cells were added to a 96-well plate for adherent growth. Mn-FSD-4 with different concentrations (0, 1.562, 3.125, 6.25 and 12.5 $\mu g \cdot mL^{-1}$) were added to the wells. After incubating for 24 h, staining HL-7702 cells and A549 cells with MTT. At last, the absorbance (A) of each well was monitored at 570 nm on a microplate reader. The cell viability was expressed as follows: cell viability=$A_{sample}/A_{control} \times 100\%$. All experiments were performed in triplicate.

1.4 Cellular uptake study

In the experiment, HL-7702 cells and A549 cells were seeded into a 6-well plate and cultured with Mn-FSD-4 (4 $mg \cdot mL^{-1}$) for 4 h. Before the confocal imaging, the cells were washed with phosphate-buffered saline (PBS) for three times. Confocal fluorescence imaging was performed on a laser scanning confocal microscope (Zeiss LSM 710).

1.5 Fluorescence imaging in mice

Nude mice were purchased from Charles River Laboratories in Beijing. All animals were kept in a constant temperature environment of 22 ℃ and keep plenty of food and water. The nude mice were injected with Mn-FSD-4 solution (total dose=100 μL, $c_{Mn\text{-}FSD\text{-}4}$=4 $mg \cdot mL^{-1}$) via intratumoral injection. After treatment for 1 h, *in vivo* fluorescence imaging was performed on an IVIS imaging system (Iumina Ⅱ)

1.6 *In vivo* biodistribution studies

Shortly, athymic nude mice were injected with Mn-FSD-4 (4 $mg \cdot mL^{-1}$) by intraperitoneal and sacrificed at time intervals of 0, 15 and 30 h. Lastly, the fluorescence signal intensities of the tissues were collected and imaged on an IVIS imaging system (Iumina Ⅱ)

1.7 *In vitro* and *in vivo* T1 MRI measurements

In vitro and *in vivo* MRI was performed on a Siemens Prisma 3.0 T MR scanner (Erlangen, Germany) with gradient strength up to 80 $mT \cdot m^{-1}$. For *in vitro* measurements, solutions with different Mn^{2+} concentrations (0, 0.062 5, 0.125, 0.25, 0.5 $mmol \cdot L^{-1}$) were tested. For *in vivo* MRI, all mice were kept in a constant temperature environment of 22 ℃ and kept plenty of food and water. The nude mice were injected with Mn-FSD-4 solution (total dose=200 μL, $c_{Mn\text{-}FSD\text{-}4}$=5 $mg \cdot mL^{-1}$) via intratumoral injection. After treatment for 4 h, *in vivo* MRI was performed.

1.8 Ethics statement

This study was performed in strict accordance with the Helsinki Declaration of 1975, as revised in 2008 (5) concerning Human and Animal Rights. All animal experiments were carried out according to the Ethical Committee of Inner Mongolia Medical University. All animal experiments were approved by Inner Mongolia Medical University.

2 Results and discussion

In general, the particle size can be adjusted via altering the reaction conditions. In this study, Mn-FSD with different sizes and morphologies were achieved under different reaction conditions. PVP and glucose was applied to control over the size and morphology of Mn-FSD. Apparently, the morphology was tuned from rodlike to irregular sphere and the sizes of Mn-FSD decreased from 10 μm to 500 nm (Fig.1). As we know, PVP and glucose are able to cover the surface of Mn-FSD. Additionally, the attachment of PVP and glucose can be acted as a structure-directing agent, inducing Mn-FSD to grow in different directions and resulting in Mn-FSD with different morphologies[21-22]. Meanwhile, XRD patterns of Mn-FSD-1, Mn-FSD-2, Mn-FSD-3 and Mn-FSD-4 were matched well with the simulated one and the sharp peaks of all the products indicate they have excellent crystallinity, as shown in Fig. 2. Thus, the decrease of the particle size did not cause the change of the Mn-FSD. The FTIR spectra of

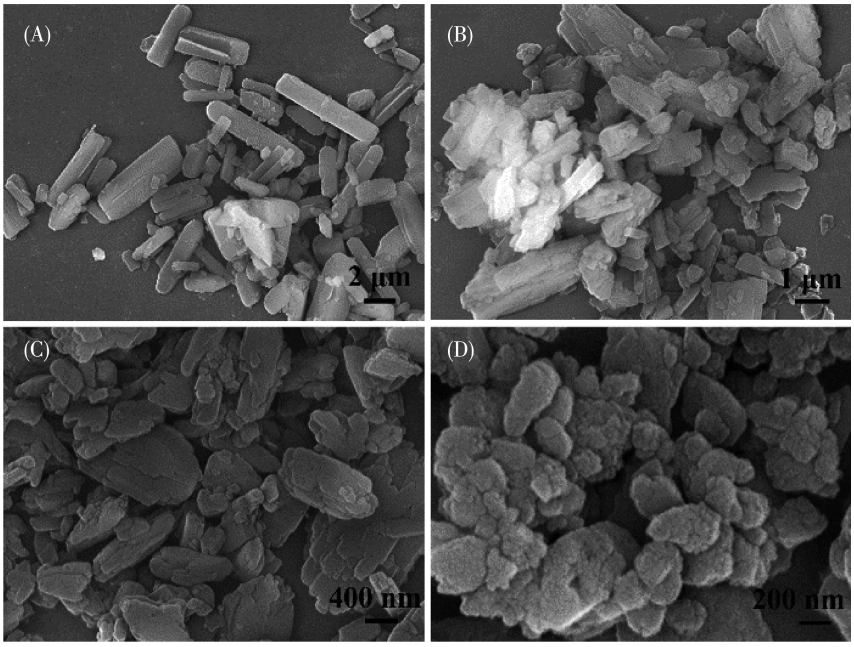

Fig.1 SEM images of Mn-FSD with different sizes and morphologies: (A) Mn-FSD-1, (B) Mn-FSD-2, (C) Mn-FSD-3, (D) Mn-FSD-4

Na_2FSD and Mn-FSD-1~Mn-FSD-4 are displayed in Fig. S1 (Supporting information). Apparently, Mn-FSD-1 ~Mn-FSD-4 exhibited almost consistent characteristic bands. Compared with Na_2FSD, the absorption bands at 1 610~1 560 cm^{-1} and 1 440~1 360 cm^{-1} attributed to —COO^- became sharp, which may be due to coordination between Mn^{2+} and —COO^- in FSD. Besides, the TGA curves of Mn-FSD-1~Mn-FSD-4 were similar. As depicted in Fig. S2, the weight loss (about 3%) occurring at 45~157 ℃ originates from the loss of solvent molecules. The significant weight loss around 330 ℃ corresponds to the collapse of frameworks of Mn-FSD-1 ~Mn-FSD-4. The solid-state UV-Vis absorption spectra are also shown in Fig.S3. Mn-FSD-1~Mn-FSD-4 exhibited an absorption maximum at 440 nm with a few shoulder peaks at 336, 500 and 613 nm. Meanwhile, fluorescence spectra are depcited in Fig. S5 and S6. Clearly, Mn-FSD-1~Mn-FSD-4 displayed emission with a maximum at 520 nm upon excitation at 445 nm, respectively. Na_2FSD exhibited a broad emission band with a maximum at 529 nm when the excitation was 361 nm as shown in Fig. S4. Obviously, the fluorescence properties of Mn-FSD-1~Mn-FSD-4 are mostly attributed to FSD. Meanwhile, the quantum efficiency of Mn-FSD-4 was 3.55%, which was higher than Na_2FSD (2.28%) due to the charge transfer interaction between Mn^{2+} and FSD[20].

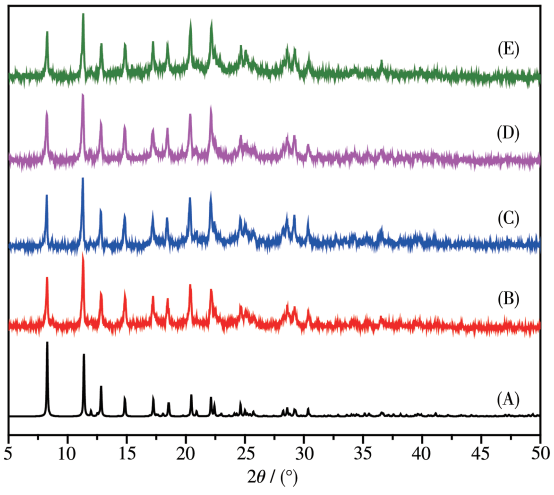

Fig.2 XRD patterns of Mn-FSD with different sizes and morphologies: (A) simulated, (B) Mn-FSD-1, (C) Mn-FSD-2, (D) Mn-FSD-3, (E) Mn-FSD-4

Besides, it is well known that the Mn^{2+} is able to serve as T_1 contrast agent and the micro-nanoscale Mn-FSD-4 was selected to confirm the MRI ability. T_1-weighted MRI of the fabricated Mn-FSD-4 are shown in inset of Fig.3. With the concentration of Mn-FSD-1 increasing, the MRI of Mn-FSD-1 gradually became brighter, demonstrating concentration-dependent signal enhancement effects. Further, the transverse relaxivity (r_1) for Mn-FSD-1 can be calculated to be 4.95 $L \cdot mmol^{-1} \cdot s^{-1}$ according to the linear concentration-depen-

dent effect in Fig.3. This value was relatively high compared with the relaxivities for most Mn-based MRI agents shown in Table S1. This may be attributed to the 2D network structure of as-prepared Mn-FSD-4, which allows the direct interaction between the Mn^{2+} and surrounding water protons and is beneficial to T_1 relaxivity. The result indicates that Mn-FSD-4 is a good T_1-weighted contrast agent for MRI. Inspired by these properties, the cell viability of Mn-FSD-4 was further explored. As shown in Fig.S7, Mn-FSD-4 displayed low cytotoxicity to HL-7702 cells and A549 cells. When the concentration was 12.5 $\mu g \cdot mL^{-1}$, the cell viability of A549 cells and HL-7702 cells was over 80% and 70%, respectively.

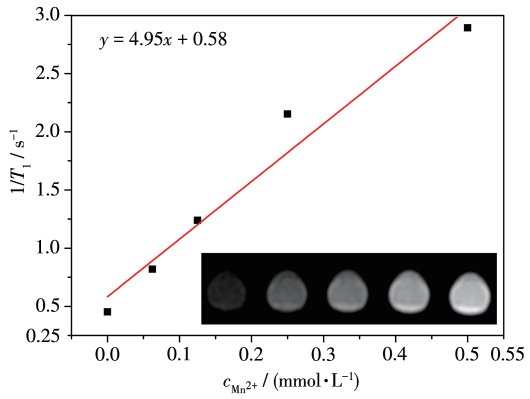

Inset: T_1-weighted MRI of Mn-FSD-4 with diverse Mn concentrations *in vitro*

Fig.3　Relaxation rate $1/T_1$ vs concentration of Mn-FSD-4 at 3.0 T and 25 ℃

Given their favorable *in vitro* cytotoxicity, we carried out fluorescence imaging tests on HL-7702 cells and A549 cells. As shown in Fig.4, bright green fluorescence can be observed in both HL-7702 cells and A549 cells after incubating with Mn-FSD-4 for 4 h, confirming that Mn-FSD-4 can enter into HL-7702 cells and A549 cells for fluorescence imaging. The bioimaging capability of Mn-FSD-4 was further investigated on the tumor bearing mice. As expected, after intratumoral injection, the tumor exhibited strong fluorescence (Fig. 5). Furthermore, *in vivo* MRI is shown in Fig. 6. Apparently, after intratumoral injection, T_1-weighted MRI displayed intense contrast enhancement and the tumor became brighter. Briefly, Mn-FSD-4 displays good OI and T_1-weighted MRI ability.

The biodistribution of Mn-FSD-4 in major organs were also investigated and are shown in Fig.7, which have a decisive influence on the possible side effects. Apparently, Mn-FSD-4 were heavily distributed in liver and kidney after intraperitoneal injection for 15 h. It is worth noting that the fluorescence intensity at liver and kidney site significantly decreased after 30 h, indicating that almost all Mn-FSD-4 were metabolized. Thus, Mn-FSD has good dispersion and fast metabo-

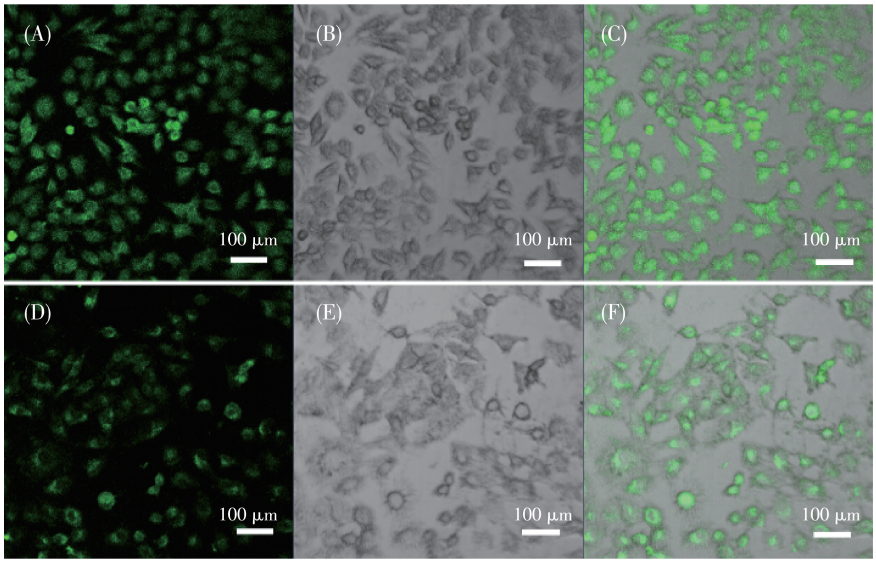

The left panels show dark-field fluorescence images, the middle panels show the corresponding bright-field images and the right panels are overlays of the left and middle panels

Fig.4　Fluorescence imaging of HL-7702 cells (A~C) and A549 cells (D~F) after being incubated with Mn-FSD-4 for 4 h

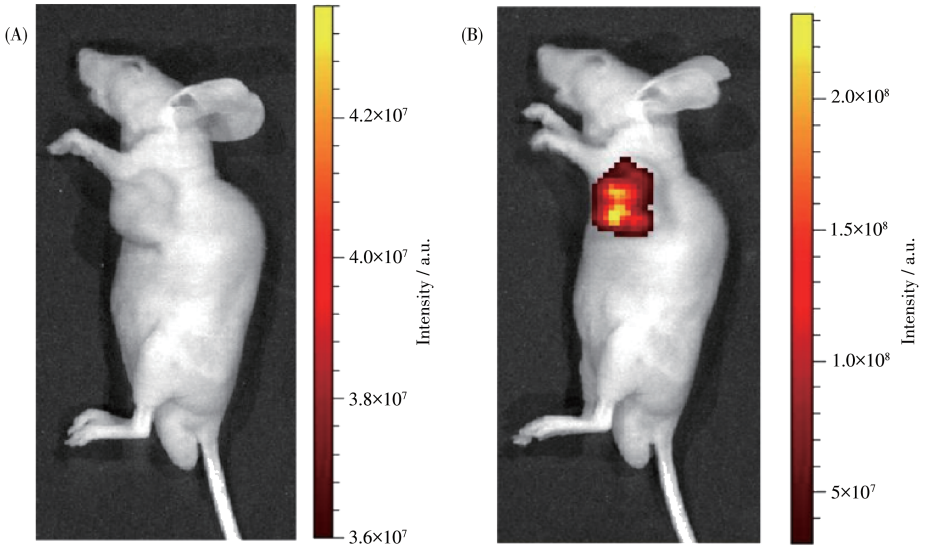

Fig.5 Fluorescence imaging of tumor-bearing athymic nude mice without Mn-FSD-4 (A) and with Mn-FSD-4 after intratumoral injection for 1 h (B)

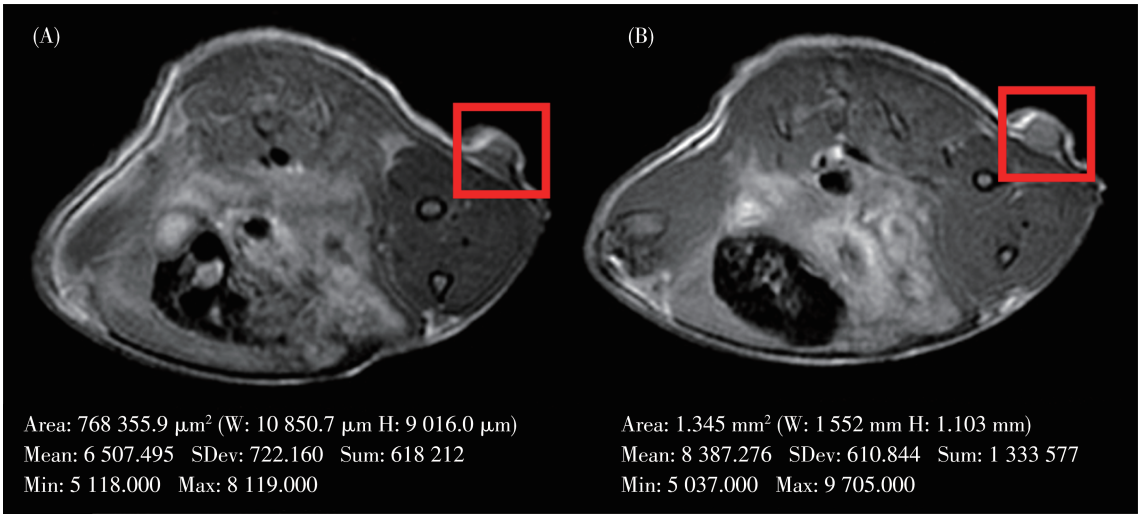

Fig.6 T_1-weighted MRI of tumor-bearing athymic nude mice without Mn-FSD-4 (A) and with Mn-FSD-4 after intratumoral injection for 4 h (B)

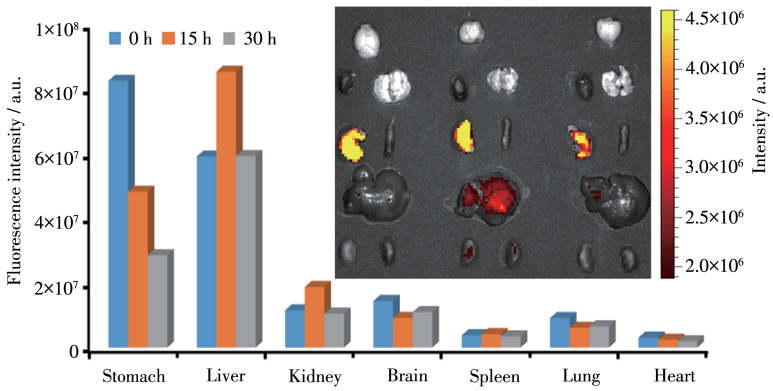

Inset: *ex vivo* fluorescence imaging of different organs at 15 and 30 h point post-injection

Fig.7 Biodistribution of Mn-FSD-4 in major organs after 15 and 30 h post-injection

lism *in vivo* applications. And the XRD of Mn-FSD after soaking for 24 h in PBS with different pH values are shown in Fig.S8. Clearly, XRD patterns of Mn-FSD after soaking in PBS with different pH values (3, 5, 7 and 8) for 24 h agreed well with the original Mn-FSD, suggesting that Mn-FSD is stable under physiological conditions.

3 Conclusions

In summary, this work shows that a novel MRI and OI bimodal probe can be developed via a simple one-pot method through the combination of metal ions with ligand for the first time. The size of Mn-FSD can be controlled to 100 nm for biological application. As expected, micro-nanoscale Mn-FSD displayed good biocompatibility. More importantly, the Mn-FSD showed high fluorescence emission at around 520 nm under the excitation of about 445 nm, effectively realizing fluorescence imaging in cell and *in vivo*. Additionally, micro-nanoscale Mn-FSD also showed high relaxivity values, exhibiting good performance in MRI. Overall, this work integrated a MOF as a novel MRI and OI dual-mode imaging reagent via a simple and gentle process. It is also expected that the methods in this work paves the way for self-assembly of multifunctional MOFs based on metal ions and organic ligands for using in biomedicine.

Conflicts of interest: There are no conflicts to declare.

Acknowledgements: This work was supported financially by the Higher Education Research Project of the Inner Mongolia Autonomous Region (Grant No.NJZY19073), Research Funds of Inner Mongolia University of Technology (Grant No.BS201909) and the Inner Mongolia Autonomous Region Fund for Natural Science (Grants No. 2019BS02010, 2020MS02014). This work was also financial support from the National Natural Science Foundation of China (Grant No.21763021). The author extends special thank to the center for new drug safety evaluation and research in Inner Mongolia Medical University.

Supporting information is available at http://www.wjhxxb.cn

References:

[1] Liu Y L, Tang Z Y. *Adv. Mater.*, **2013**,**25**:5819-5825

[2] He L C, Liu Y, Liu J Z, Xiong Y S, Zheng J Z, Liu Y L, Tang Z Y. *Angew. Chem. Int. Ed.*, **2013**,**52**:3741-3745

[3] Zhao M T, Deng K, He L C, Liu Y, Li G D, Zhao H J, Tang Z Y. *J. Am. Chem. Soc.*, **2014**,**136**:1738-1741

[4] Cohen S M. *Chem. Rev.*, **2012**,**112**:970-1000

[5] Ryder M R, Tan J C. *Mater. Sci. Technol.*, **2014**,**30**:1598-1612

[6] An H D, Li M M, Gao J, Zhang Z J, Ma S Q, Chen Y. *Coord. Chem. Rev.*, **2019**,**384**:90-106

[7] Lian X B, Xu L L, Chen M D, Wu C E, Li W J, Huang B B, Cui Y. *J. Nanosci. Nanotechnol.*, **2019**,**19**:3059-3078

[8] Lin R B, Xiang S C, Li B, Cui Y J, Qian G D, Zhou W, Chen B L. *Coord. Chem. Rev.*, **2019**,**384**:21-36

[9] Seetharaj R, Vandana P V, Arya P, Mathew S. *Arabian J. Chem.*, **2019**,**12**:295-315

[10]Zhang Z, Sang W, Xie L S, Dai Y L. *Coord. Chem. Rev.*, **2019**,**399**: 213022

[11]Wang D D, Zhou J J, Chen R H, Shi R H, Zhao G Z, Xia G L, Li R, Liu Z B, Tian J, Wang H J, Guo Z, Wang H B, Chen Q W. *Biomaterials*, **2016**,**100**:27-40

[12]Li Y T, Tang J L, He L C, Liu Y, Liu Y L, Chen C Y, Tang Z Y. *Adv. Mater.*, **2015**,**27**:4075-4080

[13]Gao X C, Zhai M J, Guan W H, Liu J J, Liu Z L, Damirin A. *ACS Appl. Mater. Interfaces*, **2017**,**9**:3455-3462

[14]Parrott D, Fernando W S, Martins A F. *Inorganics*, **2019**,**7**:18-39

[15]Erstad D J, Ramsay I A, Jordan V C, Sojoodi M, Fuchs B C, Tanabe K K, Caravan P, Gale E M. *Invest. Radiol.*, **2019**,**54**:697-703

[16]Gale E M, Atanasova I P, Blasi F, Ay I, Caravan P. *J. Am. Chem. Soc.*, **2015**,**137**:15548-15557

[17]Arhangelskis M, Eddleston M D, Reid D G, Day G M, Bučar D K, Morris A J, Jones W. *Chem. Eur. J.*, **2016**,**22**:10065-10073

[18]Zhuang J, Kuo C H, Chou L Y, Liu D Y, Weerapana E, Tsung C K. *ACS Nano*, **2014**,**8**:2812-2819

[19]Gedrich K, Heitbaum M, Notzon A, Senkovska I, Frohlich R, Getzschmann J, Mueller F, Glorius F, Kaskel S. *Chem. Eur. J.*, **2011**, **17**:2099-2196

[20]Maity K, Mukherjee D, Sen M, Biradha K. *ACS Appl. Nano Mater.*, **2019**,**2**:1614-1620

[21]Jiang D L, Xing C S, Liang X M, Shao L Q, Chen M. *J. Colloid Interface Sci.*, **2016**,**461**:25-31

[22]Bhattarai R M, Pandiyarajan S M S, Saud S, Kim S J, Mok Y S. *Dalton Trans.*, **2020**,**49**:14506-14519